# The antimicrobial peptide Defensin cooperates with Tumour Necrosis Factor to drive tumour cell death in *Drosophila*

Jean-Philippe Parvy[1]*, Yachuan Yu[1], Anna Dostalova[2], Shu Kondo[3], Alina Kurjan[5], Philippe Bulet[4], Bruno Lemaitre[2], Marcos Vidal[1] and Julia B. Cordero[1, 5]*

[1] CRUK Beatson Institute, Garscube Estate, Switchback Road, Glasgow, G61 1BD, UK

[2] Global Health Institute, School of Life Sciences, Ecole Polytechnique Federale de Lausanne, Station 19, 1015 Lausanne, Switzerland

[3] Invertebrate Genetics Laboratory, Genetic Strains Research Center, National Institute of Genetics, Mishima 411-8540, Japan

[4] Institute for Advanced Biosciences, CR University Grenoble Alpes, Inserm U1209, CNRS UMR5309, Immunologie Analytique des Pathologies Chroniques, Grenoble, France

[5] Institute of Cancer Sciences, University of Glasgow, Garscube Estate, Switchback Road, Glasgow, G61 1QH, U.K

* Corresponding Authors: j.parvy@beatson.gla.ac.uk, Julia.Cordero@glasgow.ac.uk

## Abstract

Antimicrobial peptides (AMPs) are small cationic molecules best known as mediators of the innate defence against microbial infection. While *in vitro* and

*ex vivo* evidence suggest AMPs' capacity to kill cancer cells, *in vivo* demonstration of an anti-tumour role of endogenous AMPs is lacking. Using a *Drosophila* model of tumourigenesis, we reveal a role for the AMP Defensin in the control of tumour progression. Our results reveal that Tumour Necrosis Factor mediates exposure of phosphatidylserine (PS), which makes tumour cells selectively sensitive to the action of Defensin remotely secreted from tracheal and fat tissues. Defensin binds tumour cells in PS-enriched areas, provoking cell death and tumour regression. Altogether, our results provide the first *in vivo* demonstration for a role of an endogenous AMP as an anti-cancer agent, as well as a mechanism that explains tumour cell sensitivity to the action of AMPs.

## Introduction

Vast amount of evidence demonstrates the key role of systemic immunity in tumour progression and patient outcome. Efforts to manipulate the immune response to tumours are at the core of basic and translational cancer research. In mammals and flies, tumourigenesis triggers inflammation and activation of the immune system, leading to tumour cell death (Cordero et al., 2010; Parameswaran and Patial, 2010; Parisi et al., 2014; Teng et al., 2008). Tumour Necrosis Factor (TNF) is an important player in these tumour/immune interactions and has pleiotropic effects on tumours, including induction of cell death (Ham et al., 2016; Parameswaran and Patial, 2010). This function is conserved in *Drosophila*, where the single TNF homolog Eiger (Egr), produced by tumour-associated macrophages (TAMs), has been shown

51 to drive cell death of neoplastic tumours, generated in imaginal discs by the
52 loss of apico-basal complex components such as Disc large 1, Scribble or
53 Lethal giant larvae (Cordero et al., 2010; Parisi et al., 2014; Parvy et al.,
54 2018). Moreover, using *disc large 1 Drosophila* mutant larvae (*dlg*$^{40.2}$ hereafter
55 referred to as *dlg*), we recently reported that tumour-derived Egr, acts on
56 haemocytes to activate Toll pathway in the *Drosophila* fat body, which was
57 necessary to mediate TNF-dependent tumour cell death (Parisi et al., 2014).
58 However, the mechanisms by which Toll signalling activation in immune
59 tissues executes tumour cell death remain unknown (Figure 1A).

60 In *Drosophila* as in mammals, Toll pathway is well known to play a
61 central role in the innate immune response to infection (Lemaitre et al., 1996).
62 Downstream effectors of the Toll pathway include antimicrobial peptides
63 (AMPs), which possess microbicidal activities against various pathogens.
64 They display potent antimicrobial activity *in vitro* by disrupting negatively-
65 charged microbial membranes. While intracellular activities have been
66 reported, many AMPs kill pathogens by inserting into the lipid bilayer and
67 disrupting the membrane integrity (Brogden, 2005). Host cells are instead
68 protected from AMP as they are positively charged and contain cholesterol
69 (Brender et al., 2012). *In vitro* studies have revealed AMPs capacity to kill
70 cancer cells (Deslouches and Di, 2017). However, whether this cancer-killing
71 activity is a natural function of AMPs is unknown, as there are no reports on
72 an *in vivo* paradigm addressing such question. Since the Toll pathway is
73 activated in *dlg* mutant tumour bearing larvae and is required for optimal TNF-
74 induced tumour cell death (Parisi et al., 2014), we hypothesised that AMPs
75 may be involved in this process.

76 Here we show that *Drosophila defensin* is induced in the fat body and
77 tracheal system of *dlg* mutant tumour bearing larvae. We find Defensin
78 consistently associated to dying tumour cells. Critically, systemic and tissue
79 specific knockdown of Defensin demonstrates a non-redundant role of the
80 AMP in controlling tumour growth through the induction of tumour cell death.
81 Anti-tumoural Defensin production relies on TNF-dependent activation of both
82 Toll and Imd pathway. Our results demonstrate that *dlg* mutant tumours
83 expose PS in response to haemocyte-derived TNF and that Defensin is
84 present in PS enriched area on the tumour surface. Finally, we find that lack
85 of TNF prevents tumour PS exposure and makes them insensitive to the
86 action of Defensin. Collectively, our results reveal an anti-tumoural role for
87 Defensin *in vivo* and provide insights into the molecular mechanisms, which
88 make tumours sensitive to the killing action of an endogenous AMP.
89

90 **Results**

91 ***dlg* tumour bearing larvae express the AMP Defensin**

92 In order to assess expression of several AMPs we performed RT-
93 qPCR analysis on fat bodies dissected from wild type controls ($w^{1118}$) or *dlg*
94 mutant larvae (Figure 1B). Results showed consistent and statistically
95 significant upregulation of *defensin* in fat bodies of *dlg* larvae compared to
96 wild-type ones (Figure 1B). Other Toll-dependent AMPs display a trend to be
97 increased (*drosomycin* and *attacin A*), even though data was highly variable
98 amongst biological replicates, while other AMPs were not transcriptionally
99 regulated (*drosocyn*, *cecropin A1*) (Figure 1B). Interestingly, human β-
100 Defensin 1 displays anticancer activity *in vitro* (Bullard et al., 2008; Sun et al.,

101 2006), and deletion of human *defensin* genes appears prevalent in some
102 cancer types (Ye et al., 2018). This prompted us to explore the role of
103 *Drosophila* Defensin in *dlg* mutant tumours. Using *dlg* larvae reared on
104 antibiotics, we confirmed that *defensin* upregulation was independent of the
105 presence of microbes (Figure 1C). Moreover, larvae bearing *dlg* imaginal
106 discs tumours induced by RNAi (*en>UAS-dcr2; UAS-dlg-IR*) also displayed
107 increased *defensin* expression, confirming AMP gene induction as a
108 consequence of *dlg*-driven epithelial transformation rather than whole body
109 gene loss (Figure 1D). We conclude that Defensin, an AMP known for its
110 activity against microbes, is induced, in a sterile environment, by the presence
111 of tumours.
112
113 **Defensin restrains *dlg* tumour growth and promotes tumour cell death.**
114 We next hypothesized that Defensin may be an important mediator of
115 anti-tumour immunity *in vivo*. To test this hypothesis, we generated null
116 mutant alleles for the *defensin (def)* gene using the CRISPR/Cas9 system
117 ($def^{sk3}$ and $def^{sk4}$) (Figure 1E) (Hanson et al., 2018). Survival analysis of $def^{sk3}$
118 flies confirmed that this AMP contribute to resist systemic infection to certain
119 Gram-positive bacteria (Figure supplement 1) (Levashina et al., 1995). To
120 evaluate the effect of Defensin on tumour development, we combined *def* and
121 *dlg* loss of function alleles. Compared to *dlg* mutant animals, *dlg;def* double
122 mutants displayed a significant increase in tumour size (Figure 2A). Tumour
123 growth is limited by apoptotic tumour cell death as revealed by Dcp1 staining
124 (Parisi et al., 2014). Interestingly, tumours from *dlg;def* double mutants display
125 a very strong decrease in apoptosis (Figure 2B-E'), suggesting that increased

126 tumour size in absence of Defensin is due to a decrease in tumour cell death.
127 This was further supported by the similar proliferation rates measured in *dlg*
128 and *dlg,def* mutant tumours as per quantification of anti-phophoHistone H3
129 staining (Figure supplement 2A-E'). Importantly, the effect of Def on tumour
130 size and cell death were still observed when *dlg* and *dlg,def* larvae were
131 reared in sterile conditions (Figure supplement 2F-J') and further confirmed
132 upon ubiquitous knock down of *def* using RNA interference (IR) (Figure 2F-J').
133 Furthermore, fat body overexpression of *def* significantly rescued tumour
134 volume and tumour cell death of *dlg;def*$^{sk3}$ double mutant animals (Figure 2K
135 and L). Additionally, larval injection of a synthetic Defensin peptide increased
136 tumour cell death of *dlg* or *dlg;def*$^{sk3}$ imaginal discs (Figure 2M), while it had
137 no effect on tissues from wild-type larvae, indicating that Defensin can
138 selectively promote cell death of tumour cells. Altogether, these results
139 demonstrate that Defensin is required to control *dlg*-dependent
140 tumourigenesis *in vivo* through induction of tumour cell death.
141
142 **Defensin remotely produced from immune tissues bind to tumour cells**
143 Having shown that Defensin restrict tumour growth, we sought to
144 determine the tissues that produced endogenous Defensin in the context of
145 tumour bearing. Previous studies have shown that Defensin is not produced
146 by imaginal discs or tumours (Bunker et al., 2015; Kulshammer et al., 2015).
147 In the context of infection, Defensin can be produced by the fat body as well
148 the tracheal and gut epithelium (Tzou Immunity 2000). We monitored *defensin*
149 expression by RT-qPCR in various immune tissues of tumour bearing
150 animals. We observed that the fat body, homologue to the mammalian liver

151 and adipose tissue, and the trachea, a network of tubes transporting oxygen
152 to cells that resembles the mammalian vasculature, were the main sources of
153 *defensin* in these animals (Figure 3A). This was also supported by Defensin
154 immunostaining, which detected AMP expression in the fat body (Figure 3B),
155 and tumour-associated (Figure 3C) and tumour-distant trachea (Figure 3D).
156 Transcript assessment upon targeted IR knock down of *defensin* in the
157 respective tissues further confirmed the various domains of endogenous gene
158 expression (Figure 3E and J). Importantly, knocking down *defensin*
159 expression specifically in the fat body or the trachea of *dlg* animals, resulted in
160 increased tumour size and decreased tumour cell death (Figure 3F-I' and K-
161 N') confirming the non-redundant functional requirement of *defensin* in both
162 tissues to efficiently promote tumour cell death.

163 To further investigate the possibility that Defensin produced by the fat
164 body and the trachea can specifically target tumour cells, we made use of an
165 inducible haemagglutinin (HA) tagged form of Defensin (*UAS-def-HA*). We
166 noticed leaky HA protein expression in the tracheal system of animals
167 carrying the *UAS-def-HA* construct only (Figure 4A and B), while no staining
168 was detected in tissues from wild type larvae (data not shown). Therefore,
169 expressing *UAS-def-HA* in the fat body using a Gal4 specific driver (*lpp>def-*
170 *HA*) resulted in detectable protein expression in both the trachea and the fat
171 body (Figure 4C and D). Strikingly, immunostaining revealed the presence of
172 Defensin-HA in transformed imaginal discs from *dlg* mutant animals (Figure
173 4E and E') but not in normal tissues from heterozygous animals (Figure 4F
174 and F').

175 Consistently, using anti-Defensin antibody, we observed Defensin
176 staining on *dlg* mutant tumour (Figure 4G-H'') but not in the wild-type discs
177 (Figure 4I). Interestingly, we predominantly observed Defensin bound to
178 tumour areas enriched with apoptotic cells (Figure 4H-H''). High-resolution
179 imaging showed Defensin enrichment at the membrane of these dying cells
180 (Figure 4J-J'').

181 Altogether, these results show that Defensin produced by the trachea
182 and fat body selectively binds tumour cells to target them for apoptosis.

183

184 **Toll and Imd pathway contribute to Defensin expression in *dlg* mutant**
185 **larvae**

186 *defensin* expression upon systemic infection relies on both Toll and
187 Imd pathways (Lemaitre et al., 1996; Leulier et al., 2000). While we previously
188 showed that Toll pathway activation in *dlg* mutant larvae is required to achieve
189 maximal tumour cell death (Parisi et al., 2014), the involvement of the Imd
190 pathway in tumour bearing animals was still elusive. To assess the
191 contribution of the Imd pathway to both *defensin* expression and tumour
192 burden, we analysed these two phenotypes in larvae deficient for the Imd-
193 pathway. We observed a 55-60% decrease in *defensin* expression in *dlg*
194 mutants carrying a loss of function allele affecting *imd* (*dlg;imd*$^{1}$) (Figure 5A)
195 or the gene encoding the downstream transcription factor Relish (*dlg;rel*$^{E20}$)
196 (Figure 5F). Consistently, analysis of tumour phenotypes revealed increased
197 tumour volume and decreased tumour cell death in *dlg;imd*$^{1}$ and *dlg;rel*$^{E20}$
198 animals when compared with *dlg* counterparts (Figure 5B-E' and G-J').
199 Altogether, these data demonstrate that the Imd pathway is required for

200 *defensin* upregulation, impairment of tumour growth and induction of tumour
201 cell death in *dlg* mutant larvae.

202 Upon infection, AMP expression in the trachea exclusively relies on the
203 Imd pathway (Tzou et al., 2000). We therefore looked at *defensin* expression
204 and tumour phenotype in *dlg* mutant larvae where *imd* expression had been
205 knocked down specifically within tracheal cells (*dlg;btl>imd-IR*). In this setting,
206 *defensin* expression was significantly reduced in the whole larvae (Figure 6A).
207 Consistently, tumour volume was increased while tumour cell death was
208 decreased (Figure 6B-E') showing the requirement of Imd pathway in the
209 tracheal system to control tumour burden.

210 In the fat body, both Imd and Toll patways contribute to AMPs
211 expression during infection (Tzou et al., 2002). To evaluate the contribution of
212 Toll and Imd pathways in fat body in tumour bearing larvae, we monitored
213 *defensin* expression and tumour phenotype in *dlg* animals in which Toll or Imd
214 pathways have been selectively knocked down in the fat body. Knocking
215 down *myd88,* which encodes a common adaptor to Toll receptors (Imler and
216 Zheng, 2004), or *imd* in the fat body resulted in a significant decrease in
217 *defensin* expression (Figure 6F) and, consistently, increased tumour volume
218 and decreased tumour cell death (Figure 6G-K'). Moreover, concomitant
219 overexpression of *defensin* and *Myd88-IR* or *Imd-IR* in the fat body of *dlg*
220 larvae was sufficient to significantly rescue the tumour volume and tumour cell
221 death phenotypes resulting from fat body knockdown of *Myd88* or *Imd* in *dlg*
222 animals (Figure 6L-O).

223 We conclude that, in *dlg* mutant animals, Toll and Imd pathways have
224 non-redundant roles in restricting tumour growth and promoting tumour cell

225 death through the control of *defensin* expression. Importantly, forced Defensin
226 expression in an otherwise immune-compromised animal is sufficient to
227 reduce tumour growth and to promote tumour cell death.
228

229 **Defensin is enriched in tumour areas exposing phosphatidylserine**

230 AMPs targeting of pathogens, involves the recognition of negatively
231 charged molecules exposed on the cell surface (Yeaman and Yount, 2003). A
232 key question raised by our study is how Defensin can selectively bind and kill
233 tumour cells (Figure 4 and Figure 2M). Selective action of cationic AMP is
234 attributed to their ability to interact with negative charged membrane such as
235 those found in bacteria. We hypothesized that the membrane of tumour cells
236 from *dlg* mutant larvae might change their electrostatic properties, making
237 them sensitive to the action of Defensin. Phosphatidylserine **(**PS) is a
238 negatively charged phospholipid, normally restricted to the inner leaflet of the
239 cell membrane. However, PS can be exposed on the outer leaflet for example
240 in apoptotic cells, which tags these cells for phagocytosis (Birge et al., 2016;
241 Shklyar et al., 2013; Tung et al., 2013). Moreover, PS exposure has been
242 shown to occur independently of apoptosis in many cancer cell types (Riedl et
243 al., 2011). Therefore, we investigated whether PS externalisation could be a
244 factor allowing specific targeting of tumour cells by Defensin. Our data
245 revealed that *dlg* but not wild-type tissues, displayed high levels of Annexin V
246 staining (Figure 7A and B), indicating increased exposure of PS by *dlg*
247 tumours. We next looked at the ability of Defensin to specifically associate
248 with tumour cells exposing PS and found that Defensin localized in PS-
249 enriched areas on *dlg* tumours (Figure 7A-A''). Thus, Defensin produced by

250 immune responsive tissues binds specifically to tumour cells and this ability
251 correlated with the exposure of PS.
252
253 **The TNF homolog Eiger is required for PS exposure and Defensin anti-**
254 **tumoural activity.**
255 Previous studies have shown that circulating macrophage-like cells in
256 *Drosophila,* called haemocytes, bind to *dlg* mutant tumours and contribute to
257 cell death (Parisi et al., 2014). This process is mediated by the release of Egr
258 from haemocytes (Cordero et al., 2010; Parisi et al., 2014), which then
259 activates the JNK pathway in target cells to promote apoptosis (Igaki et al.,
260 2009). Moreover, Toll pathway–activation in tumour bearing animals also
261 requires Egr (Parisi et al., 2014). Accordingly, we found that *defensin*
262 upregulation observed in *dlg* animals was lost in *dlg;egr*$^{3}$ double mutants
263 (Figure 7C). We next tested whether PS exposure in tumours was dependent
264 on Egr, and observed an almost complete loss of cell-surface PS in *dlg;egr*$^{3}$
265 tumours (Figure 7A, D and E). Therefore, Egr is required for PS exposure in
266 these tumours. We then analysed PS exposure in *dlg* mutant tumours, upon
267 specific *egr* knockdown in haemocytes (*dlg;hml>egr-IR*), and observed a
268 strong decrease in cell surface-exposed PS compared to control tumours
269 (*dlg;hml>ctrl-IR*) (Figure 7F-H). This indicates that PS exposure in tumour
270 cells is likely triggered by the release of Egr from haemocytes.
271 Importantly, Egr-dependent signalling and PS exposure were intact in *dlg;def*
272 and *dlg;imd* mutants (Figure 7I-L and Figure supplement 3). This indicates
273 that Egr signalling and PS exposure precedes the action of Defensin in *dlg*
274 tumours. To further assess whether Egr was required for Defensin-induced

275 tumour cell death, we injected synthetic Defensin peptide into control, *dlg* or
276 *dlg;egr*$^{3}$ mutant larvae. As expected, Defensin injection was able to robustly
277 promote tumour cell death in *dlg* mutant tumours (Figure 7M). However,
278 Defensin was unable to affect tumours derived from Egr-deficient animals,
279 demonstrating the requirement of Egr for tumour cell death induced by
280 Defensin (Figure 7M).
281
282 **Discussion**
283 While the role of antimicrobial peptides in innate immune defense has been
284 well-recognized for decades (Bahar and Ren, 2013), recent reports revealed
285 potential additional physiological functions of AMPs. including aging and
286 neurodegeneration (Cao et al., 2014; Kounatidis et al., 2017; Lezi et al.,
287 2018), wound-healing (Chung et al., 2017; Tokumaru et al., 2005), resistance
288 to oxidative stress (Mergaert et al., 2017; Zhao et al., 2011), immune signaling
289 (Tjabringa et al., 2003; van Wetering et al., 2002) and anti-cancer activity
290 (Deslouches and Di, 2017). However, due to the absence of AMP mutants,
291 most of these studies have relied on the use of exogenous sources of AMPs
292 or genetic modification of upstream regulators of AMP expression. Recently,
293 the use of loss of function alleles of *Drosophila* Diptericin (DptB), allowed to
294 establish a role for the AMP in long-term memory (Barajas-Azpeleta et al.,
295 2018). Pioneer work reporting systematic deletion of multiple AMPs in
296 *Drosophila*, opens the door for in-depth analysis of the endogenous functions
297 of these molecules (Hanson et al., 2018). Using such tools and a genetically
298 defined *in vivo* tumour model, our study demonstrates a role for Defensin in
299 the control of tumours and deciphers the molecular mechanism allowing

300 specific tumour cell targeting by the AMP. Collectively, our results suggest a
301 model of tumour control in two steps: Firstly, the cellular immune response to
302 tumours involves the binding of haemocytes to tumour cells and activation of
303 TNF pathway leading to PS exposure (Figure 7N). This is followed by a
304 humoral response achieved by the action of antimicrobial peptides remotely
305 produced by the fat body and the trachea (Figure 7N). Thus, the two branches
306 of *Drosophila* innate immunity contribute to tumour elimination.
307

308 **A role for a *Drosophila* AMP in tumour control**

309 Using mutants as well as ubiquitous or targeted knockdowns, our study
310 reveals that Defensin is non-redundantly required to drive tumour cell death
311 and restrict tumour growth in neoplastic tumours generated by loss the apico-
312 basal determinant Dlg. This was reinforced by detection of Defensin on dying
313 tumour cells as well as genetic rescue and injection experiments showing that
314 Defensin can actively drive tumour cell death. Several *in vitro* studies in
315 mammals have shown AMPs anti-tumoural potential (Deslouches and Di,
316 2017). Amongst these suggested anticancer peptides, Human β-Defensin 1
317 (hBD1) appears downregulated in 82% of prostate cancer and in 90% of renal
318 clear cell carcinomas (Donald et al., 2003), and expression of hBD1 induces
319 cell death in prostate and renal cancer cells *in vitro* (Bullard et al., 2008; Sun
320 et al., 2006). Moreover, a recent report shows prevalent deletion of Human
321 *defensin* gene cluster in some tumour types including prostate, lung and
322 colorectal cancers, as well as a decrease overall survival in patients carrying
323 these deletions (Ye et al., 2018). However, since the classification of a
324 molecule as AMP is based on structural protein features, it is important to

325 mention that Human Defensins are not homologous of, but rather have
326 structural resemblances to Drosophila AMPs due to convergent evolution
327 (Shafee et al., 2017). Further studies are required to determine if anticancer
328 activity displayed by Defensins from different species is linked to their
329 structural properties.

330 As upon infection (Tzou et al., 2000), we show that the fat body and the
331 trachea are the main sources of Defensin in tumours bearing larvae.
332 Moreover, our results indicated that Defensin's maximal expression, and anti-
333 tumour properties rely on Imd and Toll pathways activation. As expected from
334 previous studies on anti-pathogenic immunity, Imd appears to play a critical
335 role in the tracheal system, while both Imd and Toll drive Defensin expression
336 in the fat body (Hoffmann and Reichhart, 2002; Tzou et al., 2002).
337 Consistently, overexpressing Defensin partially rescued the effect of Imd or
338 Toll knockdown on *dlg* tumours. However, Toll and Imd pathways are major
339 regulators of multiple AMPs in the *Drosophila* fat body. Then, it is conceivable
340 that AMPs other than Defensin may possess similar anti-tumoural activity. In
341 fact, a recent study in *Drosophila* shows that ectopic expression of several
342 antimicrobial peptides, including the Defensin, can increase cell death in a
343 haematopoietic tumour model (Araki et al., 2018). Authors also reported
344 activation of Toll and Imd pathways together with increased expression of
345 several AMPs in those tumour bearing animals. Together with our study, this
346 suggests a general anti-tumoural propertie of *Drosophila* AMPs.

347

348 **Defensin specifically targets tumour cells**

349 Importantly, we show that Defensin targets tumour cells for apoptosis
350 while sparing normal cells. As their human counterparts, we show that
351 *Drosophila* tumours can expose PS independently of cell death (Riedl et al.,
352 2011). Interestingly, an *in vitro* study showed selective anticancer activity of
353 some synthetic peptides derived from beetle Defensin against cancer cells
354 exposing PS (Iwasaki et al., 2009). A similar targeting mechanism has also
355 been proposed to explain temporin-1CEa or L-K6 anticancer activities towards
356 melanoma cells and breast cancer cells respectively (Wang et al., 2016;
357 Wang et al., 2017). PS is a mark of apoptotic cells, which is used as an "eat
358 me" signal by phagocytes (Shklyar et al., 2013; Tung et al., 2013). In
359 *Drosophila*, the phagocytic receptor Simu together with Draper contribute to
360 the elimination of apoptotic to the recognition of PS (Shklyar et al., 2013; Tung
361 et al., 2013). It would be interesting to test the role of these receptors in the
362 control of *dlg* tumour progression.

363 Our results indicate that PS exposure precedes Defensin action and is
364 not just an "eat-me" signal but likely contributes to changing the membrane of
365 tumour cells making them sensitive to the action of AMPs. It is tempting to
366 speculate that deleterious effect of AMPs observed upon aging or
367 neurodegeneration may involve a similar targeting mechanism of 'foreign-
368 looking' or unfit cells (Cao et al., 2013; Kounatidis et al., 2017; Lezi et al.,
369 2018). However, in this case, the immune system might rather accelerate
370 disease by promoting loss of important cell type.

371 Noteworthy, other negatively charged molecules enriched on tumour
372 surface such as heparan sulfates and O-glycosylated mucins may also

373 contribute to the targeting by AMPs (Hollingsworth and Swanson, 2004;
374 Knelson et al., 2014).
375
376 **Defensin action requires TNF**
377 TNF is a major player in the tumour microenvironment by exerting
378 pleiotropic effects on both the tumour and its surroundings (Ham et al., 2016;
379 Parameswaran and Patial, 2010). In our *dlg* mutant model, we observed that
380 defensin induction requires TNF supporting previous observations that
381 induction of innate immune response in tumour bearing animal relied on Egr
382 produced by the tumour (Parisi et al., 2014). Indeed, Toll activation in the fat
383 body has been proposed to be a consequence of tumour-derived TNF that
384 drives haemocyte proliferation leading to an increase in Toll ligand Spatzle
385 (Parisi et al., 2014). Whether Imd pathway is also indirectly activated by the
386 changes in immune cell activity in response to tumour or by alternative
387 mechanisms remains an open question.
388 Our results show that haemocyte-derived TNF is required for PS
389 exposure by the tumour, a key process for tumour targeting by Defensin.
390 Consistently, haemocyte-derived TNF is shown to drive cell death in *dlg*
391 mutant tumours (Parisi et al., 2014). The precise molecular mechanisms
392 driving PS exposure downstream of TNF remain unknown. However,
393 haemocyte-derived TNF, through TNF receptor, activates JNK pathway,
394 which triggers many changes in tumour cells including apoptosis (Igaki et al.,
395 2002; Moreno et al., 2002), ROS production (Fogarty et al., 2016;
396 Santabarbara-Ruiz et al., 2015), loss of cell polarity (Zhu et al., 2010),
397 modification of extracellular matrix (Uhlirova and Bohmann, 2006),

398 proliferation and cell migration (Beaucher et al., 2007; Igaki et al., 2006;
399 Pastor-Pareja et al., 2004; Srivastava et al., 2007). Thus, TNF might also
400 sensitize cells through activation of the JNK pathway (Cordero et al., 2010)
401 providing, in addition to PS exposure, a secondary sensitization of tumour
402 cells to the action of the AMP. Further studies are needed to explore a
403 potential link between JNK activation and PS exposure since pleiotropic
404 effects of JNK may drive PS exposure downstream of TNF.

405 Another consequence of TNF-dependent JNK activation in tumours is
406 the increased expression of matrix metalloproteases (Mmps) by tumour cells
407 (Uhlirova and Bohmann, 2006). Importantly, we show that Mmp-1 induction
408 and then JNK pathway activation are still present in tumour from larvae
409 devoided of Defensin. This demonstrates that TNF signalling acts upstream of
410 Defensin. Mmps degrade the basal membrane facilitating metastasis of
411 primary tumour cells (Beaucher et al., 2007; Pastor-Pareja et al., 2004;
412 Srivastava et al., 2007). Interestingly, a study reported that human Mmp-7 can
413 cleave immature Defensins, promoting their activation (Wilson et al., 1999;
414 Wilson et al., 2009). Indeed, the pro-domain present in AMPs is thought to
415 keep their *in vivo* activity silent, allowing local activation of AMP upon
416 cleavage. While the mechanisms of *Drosophila* Defensin pro-domain
417 cleavage remain unknown, it would be interesting to explore whether the
418 changes in the tumour microenvironment could also affect Defensin
419 activation.

420

421 In conclusion, our study provides the first direct *in vivo* demonstration of the
422 role of an endogenous AMP as an anti-cancer agent in *Drosophila*. Our data

423 points to a conserved mechanism of tumour control by AMPs, a potent arm of
424 the innate immune system. Importantly, we identify cellular features within
425 tumours, which may be predictive of their sensitivity to be targeted by AMPs.
426 This study provides a new paradigm to decipher the molecular mechanisms
427 influencing anti-tumoural functions of an AMP, which may extend to other
428 non-canonical roles of AMPs, such as in ageing, long-term memory and
429 wound healing. Moreover, together with the new genetic tools allowing
430 targeting of all *Drosophila* AMPs (Hanson et al., 2018), our study establishes
431 new bases to explore *in vivo* a potential important natural mechanism of
432 defence against tumours.
433

434 **Material and Methods**

435 ***Drosophila* housekeeping and rearing**

436 Flies were reared at 25°C under 12h/12h light/dark cycles on standard
437 oatmeal and molasses medium (Fernandez-Ayala et al., 2009). Details on fly
438 strains used in this study are presented in Table supplement 1 and detailed
439 genotypes are included in corresponding figure legends.

440 For assessment of tumour volume and tumour cell death, flies were
441 transferred to medium embryo collection cages and allowed to lay eggs for 8h
442 at room temperature (RT) on agar/grape juice plates (2.1% agar, 25% grape
443 juice, 1.25% sucrose, 0.2% methyl 4-hydroxybenzoate) supplemented with
444 yeast paste. Plates were kept at 25°C until hatching. 200 larvae hatched
445 within a 4h time window were collected and transferred to rearing bottles
446 containing 45mL of fly food to avoid any developmental delay and/or
447 starvation effects due to overcrowding conditions. The tumour phenotype was

448 analysed close to the normal developmental time, i.e. 7 days after hatching.
449 Tumours were dissected and stained for further analysis (see below).
450
451 **Generation of *defensin* mutants**
452 *def*$^{sk3}$ and *def*$^{sk4}$ mutants were generated using CRISPR/cas9
453 technology (Hanson et al., 2018). Mutants were isogenized through
454 backcrosses with a *w*$^{1118}$ *iso* line as previously described in Ferreiera-Teixeira
455 et al, 2014.
456
457 **Survival assays**
458 Survival of *def*$^{SK3}$ animals was compared to wild type controls
459 (isogenised background, *iso*). Male flies (5-7 days old) were pricked in the
460 thorax with a needle dipped in a concentrated pellet of fresh overnight
461 bacterial culture. Infected flies were kept at 29°C. *Listeria innocua* was
462 cultured in Brain heart infusion medium at 37°C and used at optical density of
463 200nm ($OD_{600}$). *Erwinia carotovora carotovora 15* was cultured in Luria-
464 Bertani broth at 29°C and used at $OD_{600}$ 200. Experiments were repeated
465 three times independently and one representative experiment is shown.
466
467
468 **Immunohistochemistry**
469 Tissues were dissected in Phosphate Buffer Saline (PBS) and fixed for
470 20min in 4% formaldehyde. Fat body samples were fixed for 30min using the
471 same protocol. Tissues were washed three times in PBS containing 1% of
472 Triton-X100 (PBT) and incubated overnight at 4°C with primary antibodies.

473 Tissues were washed 5 times in PBT and incubated for 2h at RT with
474 secondary antibodies and 4',6-Diamidine-2′-phenylindole dihydrochloride
475 (DAPI, Sigma) (1µg/mL). After three washes in PBT, tissues were mounted in
476 Vectashield (Vector Laboratories, Inc.) using Secured-Seal spacers (Thermo
477 Fisher Scientific).

478 The following primary antibodies and corresponding dilutions were
479 used: rabbit anti-Dcp1 (1/100), rabbit anti-phosphoHistone H3 (ser10 and
480 ser28 mixed, 1/100) and mouse anti-HA (1/1000) (Cell Signalling
481 Technology); mouse anti-Mmp1 (1/10) (Developmental Studies Hybrydoma
482 Bank, 3B8D12); chicken anti-GFP (1/4000) Abcam) and guinae pig anti-
483 Defensin (1/100) (Kind gift from Dahua Chen, (Ji et al., 2014)). Secondary
484 goat antibodies were Alexa Fluor® 488nm or 594nm (Invitrogen) conjugated
485 and were used at 1/500 dilution.

486 Confocal images were captured using a Zeiss 710 or Zeiss 880 with
487 Airyscan confocal microscope and processed with Fiji 2.0.0 or Adobe
488 Photoshop C.S5.1.

489

490 **Quantification of tumour volume and tumour cell death**

491 For analysing tumour phenotype, images were acquired using optimal
492 slice parameter and 12bits using a Zeiss 710 confocal microscope.
493 Quantifications were made as previously described (Parisi et al., 2014).
494 Briefly, we used Volocity 3D imaging analysis software (Perkin Elmer) to
495 quantify the total volume of tumour identified by DAPI staining and cell death
496 visualised with anti-Dcp1 staining. When haltere or leg discs tumours were
497 still associated with the wing disc, they were not considered for quantification.

498 Quantifications were done in at least three independent biological replicates
499 for each genetic setting. Single representative experiments are presented
500 except for *dlg;def* double mutant rescue experiments (Figure 1L-M) for which
501 replicates are pooled due to the few larvae available. In all cases the
502 difference between control and mutant tumour were strongly reproducible
503 between replicates.
504
505 **Sterile rearing conditions**
506 To rule out any effect of infection on the tumour phenotypes,
507 *Drosophila* larvae were reared on standard food supplemented with penicillin
508 and streptomycin (100 IU/ml and 100 mg/ml, respectively) (Figure 1A, Figure
509 supplement 3A-E' and Figure supplement 4G).
510
511 **qRT-PCR analysis**
512 Total RNA from 7 to 10 whole larvae or tissues collected from 10 to 20
513 larvae (10 larvae for fat body, 20 larvae for trachea) was extracted using
514 TRIzol (Thermo Fisher Scientific), according to the manufacturer's
515 instructions. RNA was treated with Turbo DNA free Kit (Life Technologies
516 LTD) and RNA concentration and quality were monitored using a Nanodrop
517 (Thermo Fisher Scientific). The same amount of total RNA (1µg for whole
518 larvae and fat body or 100ng for trachea) was used to perform the three
519 independent reverse-transcriptions using the High-Capacity cDNA Reverse
520 Transcription Kit (Applied Biosystems). cDNAs were pooled and qPCR was
521 performed using PerfeCTa SYBR green (Quanta Bio), following the
522 manufacturer's instructions. cDNA amplification was monitored with Applied

523 Biosystems 7500 fast instruments. Serial 10-fold dilutions of an external
524 standard were used to produce a standard curve, and RNA samples were
525 included to control for the absence of DNA contamination. *rpl32* expression
526 was used to normalize expression levels of target genes. Data was analysed
527 using the Ct method ($2^{-\Delta\Delta ct}$). All qPCR experiments were carried out on three
528 to seven independent biological replicates (see figure legends for details) and,
529 larvae were sampled from the same bottle used to analyse the tumour
530 phenotype. GraphPad Prism7 software was used for graphical representation
531 and statistical analysis. Primer targets and sequences are presented in Table
532 supplement 2.
533

534 **PCR amplification of genomic DNA**

535 To verify the sequence of *def*$^{sk3}$ and *def*$^{sk4}$ mutants, genomic DNA was
536 extracted from single flies by grinding whole animals with a 200µL pipette tip
537 containing 50µL of squishing buffer (10mM Tris-HCl pH 8.2, 1mM EDTA,
538 25mM NaCl, 200µg proteinase K) followed by incubation at 37°C for 30min.
539 Proteinase K was heat-inactivated at 95°C for 2min. 1µL of genomic DNA was
540 used for PCR amplification using PfuUltra II Fusion DNA Polymerase (Agilent)
541 (for primers see Table supplement 2) and Eppendorf Mastercycler Ep
542 Gradient Thermal Cycler.
543

544 **Annexin V staining and quantification**

545 Tumours were dissected in PBS and incubated in Annexin V binding
546 buffer (Fisher Scientific) containing 5% of Alexa Fluor (488nm or 568nm)
547 conjugated Annexin V (Life Technologies LTD) for 10min. Tissues were

548 washed quickly in Annexin V binding buffer and fixed in 4% formaldehyde for
549 20min. Immunostaining, mounting and imaging were then carried out as
550 described above.

551 We used Fiji 2.0.0 software to quantify Annexin V staining at the
552 tumour surface. Maximal Z-projection of whole tumours were generated and
553 the Colour Threshold tool was then used to detect the red pixels that
554 represented Annexin V staining at the surface of tumours. The hue slider was
555 set to include only the red signal, and the brightness slider was adjusted to
556 exclude any background signal. This area was then selected and measured in
557 pixels.

558

559 **Synthetic Defensin production and injections**

560 The mature Defensin peptide
561 (ATCDLLSKWNWNHTACAGHCIAKGFKGGYCNDKAVCVCRN) was
562 synthesised (over 90% purity) and the purity controlled by Genepep using
563 Ultra Performance Liquid Chromatography/ Mass Spectrometry. We
564 subsequently compared the integrity of synthetic Defensin with authentic
565 Defensin purified from *Drosophila* hemolymph using two complementary
566 approaches, namely Matrix-Assisted Laser Desorption/Ionization-Mass
567 Spectrometry (MALDI-MS) for molecular mass determination and trypsin
568 digestion followed by nanoLiquid Chromatography/Electrospray Ionization
569 tandem Mass Spectroscopy (nano*LC/ESI MS/MS*) for molecular integrity
570 confirmation. Those analyses confirmed the similar mass between natural and
571 synthetic Defensin (respectively provided by Bulet EIRL and Genepep) as well

572 the presence of disulphide bonds within synthetic Def, demonstrating it is the
573 mature peptide (Data not shown).

574 For injection experiments, larvae were collected, washed three times in
575 cold sterile PBS and injected on a fly pad (Flystuff-SLS UK) upon $CO_2$
576 anaesthesia using Nanoject II and glass capillaries 3.5 inch (Drummond).
577 Larvae were injected with 69nL of PBS containing 7.5nmol of synthetic
578 Defensin or 69nL of PBS only as control. Larvae were then gently transferred
579 into agar/grape juice plates and kept at 25°C. Tumours were dissected 4h
580 after injection and stained for visualization of nuclei and tumour cell death as
581 describe above.

582

583 **Statistical analyses**

584 All data are presented as mean ± SD and n values are indicated in the
585 figure legends. Statistical analyses were carried out using GraphPad Prism7
586 software and only significant differences are indicated in dot-plots. Survival
587 upon infection was analysed using Log-rank test. qPCR data were analysed
588 using unpaired t-test with a two-tailed p value. Tumour volume and tumour
589 cell death comparing 2 samples were analysed using Mann-Whitney test with
590 a two-tailed p value and the one comparing 3 genotypes were analysed using
591 One-way ANOVA followed by Turkey's multiple comparisons test. Tumour
592 volume from injected larvae was analysed using Two-way ANOVA followed by
593 Turkey's multiple comparisons test and only significant statistical differences
594 between ctrl and Defensin injected larvae for each genotype tested are
595 indicated.

596

597 **Acknowledgments:** We would like to thank Dr. Dahua Chen for the anti-
598 Defensin antibody, the Vienna *Drosophila* Resource Centre and the
599 Bloomington *Drosophila* Stock Centre for fly stocks, and Dr. Sébastien Voisin
600 for his critical contribution in mass spectrometry analyses. JPP and YY are
601 supported by Cancer Research UK core funding through the CRUK Beatson
602 Institute (A17196). JBC is a Sir Henry Dale Fellow jointly funded by the
603 Wellcome Trust and the Royal Society (grant number 104103/Z/14/Z). *In*
604 *memory of Marcos Vidal (1974-2016).*
605
606
607 **Author contributions:** MV initiated this project. JPP performed most of the
608 experiments in this study; YY and AK provided technical assistance; AD
609 assayed fly survival upon infection; SK and BL generated the *defensin* mutant
610 flies; PB analysed the quality of synthetic Def; JPP and JBC designed
611 experiments and analysed the data; BL provided important insights into AMPs
612 and *Drosophila* immunity; JPP, PB, BL and JBC wrote the paper; JBC
613 directed the study.
614
615 **Competing interests:** Authors declare no competing interests.
616
617 **Data and material availability:** All data and materials supporting the findings
618 of this study are available from the corresponding authors upon request.
619
620

621 **References**


622 Araki, M., Awane, R., Sato, T., Ohkawa, Y., and Inoue, Y. (2018). Anti-tumor effects
623 of antimicrobial peptides, targets of the innate immune system, against
624 hematopoietic tumors in Drosophila mxc mutants. BioRxiv.
625 Bahar, A.A., and Ren, D. (2013). Antimicrobial peptides. Pharmaceuticals (Basel)
626 *6*, 1543-1575.
627 Barajas-Azpeleta, R., Wu, J., Gill, J., Welte, R., Seidel, C., McKinney, S., Dissel, S., and
628 Si, K. (2018). Antimicrobial peptides modulate long-term memory. PLoS Genet
629 *14*, e1007440.
630 Beaucher, M., Hersperger, E., Page-McCaw, A., and Shearn, A. (2007). Metastatic
631 ability of Drosophila tumors depends on MMP activity. Dev Biol *303*, 625-634.
632 Birge, R.B., Boeltz, S., Kumar, S., Carlson, J., Wanderley, J., Calianese, D., Barcinski,
633 M., Brekken, R.A., Huang, X., Hutchins, J.T.*, et al.* (2016). Phosphatidylserine is a
634 global immunosuppressive signal in efferocytosis, infectious disease, and cancer.
635 Cell Death Differ *23*, 962-978.
636 Brender, J.R., McHenry, A.J., and Ramamoorthy, A. (2012). Does cholesterol play a
637 role in the bacterial selectivity of antimicrobial peptides? Front Immunol *3*, 195.
638 Brogden, K.A. (2005). Antimicrobial peptides: pore formers or metabolic
639 inhibitors in bacteria? Nat Rev Microbiol *3*, 238-250.
640 Bullard, R.S., Gibson, W., Bose, S.K., Belgrave, J.K., Eaddy, A.C., Wright, C.J., Hazen-
641 Martin, D.J., Lage, J.M., Keane, T.E., Ganz, T.A.*, et al.* (2008). Functional analysis of
642 the host defense peptide Human Beta Defensin-1: new insight into its potential
643 role in cancer. Mol Immunol *45*, 839-848.
644 Bunker, B.D., Nellimoottil, T.T., Boileau, R.M., Classen, A.K., and Bilder, D. (2015).
645 The transcriptional response to tumorigenic polarity loss in Drosophila. Elife *4*.
646 Cao, J., Ni, J., Ma, W., Shiu, V., Milla, L.A., Park, S., Spletter, M.L., Tang, S., Zhang, J.,
647 Wei, X.*, et al.* (2014). Insight into insulin secretion from transcriptome and
648 genetic analysis of insulin-producing cells of Drosophila. Genetics *197*, 175-192.
649 Cao, Y., Chtarbanova, S., Petersen, A.J., and Ganetzky, B. (2013). Dnr1 mutations
650 cause neurodegeneration in Drosophila by activating the innate immune
651 response in the brain. Proc Natl Acad Sci U S A *110*, E1752-1760.
652 Chung, E.M.C., Dean, S.N., Propst, C.N., Bishop, B.M., and van Hoek, M.L. (2017).
653 Komodo dragon-inspired synthetic peptide DRGN-1 promotes wound-healing of
654 a mixed-biofilm infected wound. NPJ Biofilms Microbiomes *3*, 9.
655 Cordero, J.B., Macagno, J.P., Stefanatos, R.K., Strathdee, K.E., Cagan, R.L., and Vidal,
656 M. (2010). Oncogenic Ras diverts a host TNF tumor suppressor activity into
657 tumor promoter. Dev Cell *18*, 999-1011.
658 Deslouches, B., and Di, Y.P. (2017). Antimicrobial peptides with selective
659 antitumor mechanisms: prospect for anticancer applications. Oncotarget.
660 Donald, C.D., Sun, C.Q., Lim, S.D., Macoska, J., Cohen, C., Amin, M.B., Young, A.N.,
661 Ganz, T.A., Marshall, F.F., and Petros, J.A. (2003). Cancer-specific loss of beta-
662 defensin 1 in renal and prostatic carcinomas. Lab Invest *83*, 501-505.
663 Fernandez-Ayala, D.J., Sanz, A., Vartiainen, S., Kemppainen, K.K., Babusiak, M.,
664 Mustalahti, E., Costa, R., Tuomela, T., Zeviani, M., Chung, J.*, et al.* (2009).
665 Expression of the Ciona intestinalis alternative oxidase (AOX) in Drosophila
666 complements defects in mitochondrial oxidative phosphorylation. Cell Metab *9*,
667 449-460.

668 Fogarty, C.E., Diwanji, N., Lindblad, J.L., Tare, M., Amcheslavsky, A., Makhijani, K.,
669 Bruckner, K., Fan, Y., and Bergmann, A. (2016). Extracellular Reactive Oxygen
670 Species Drive Apoptosis-Induced Proliferation via Drosophila Macrophages. Curr
671 Biol *26*, 575-584.
672 Ham, B., Fernandez, M.C., D'Costa, Z., and Brodt, P. (2016). The diverse roles of
673 the TNF axis in cancer progression and metastasis. Trends Cancer Res *11*, 1-27.
674 Hanson, M.A., Dostalova, A., Ceroni, C., Poidevin, M., Kondo, S., and Lemaitre, B.
675 (2018). Synergy and remarkable specificity of antimicrobial peptides in vivo
676 using a systematic knockout approach. BioRxiv.
677 Hoffmann, J.A., and Reichhart, J.M. (2002). Drosophila innate immunity: an
678 evolutionary perspective. Nat Immunol *3*, 121-126.
679 Hollingsworth, M.A., and Swanson, B.J. (2004). Mucins in cancer: protection and
680 control of the cell surface. Nat Rev Cancer *4*, 45-60.
681 Igaki, T., Kanda, H., Yamamoto-Goto, Y., Kanuka, H., Kuranaga, E., Aigaki, T., and
682 Miura, M. (2002). Eiger, a TNF superfamily ligand that triggers the Drosophila
683 JNK pathway. EMBO J *21*, 3009-3018.
684 Igaki, T., Pagliarini, R.A., and Xu, T. (2006). Loss of cell polarity drives tumor
685 growth and invasion through JNK activation in Drosophila. Curr Biol *16*, 1139-
686 1146.
687 Igaki, T., Pastor-Pareja, J.C., Aonuma, H., Miura, M., and Xu, T. (2009). Intrinsic
688 tumor suppression and epithelial maintenance by endocytic activation of
689 Eiger/TNF signaling in Drosophila. Dev Cell *16*, 458-465.
690 Imler, J.L., and Zheng, L. (2004). Biology of Toll receptors: lessons from insects
691 and mammals. J Leukoc Biol *75*, 18-26.
692 Iwasaki, T., Ishibashi, J., Tanaka, H., Sato, M., Asaoka, A., Taylor, D., and
693 Yamakawa, M. (2009). Selective cancer cell cytotoxicity of enantiomeric 9-mer
694 peptides derived from beetle defensins depends on negatively charged
695 phosphatidylserine on the cell surface. Peptides *30*, 660-668.
696 Ji, S., Sun, M., Zheng, X., Li, L., Sun, L., Chen, D., and Sun, Q. (2014). Cell-surface
697 localization of Pellino antagonizes Toll-mediated innate immune signalling by
698 controlling MyD88 turnover in Drosophila. Nat Commun *5*, 3458.
699 Knelson, E.H., Nee, J.C., and Blobe, G.C. (2014). Heparan sulfate signaling in
700 cancer. Trends Biochem Sci *39*, 277-288.
701 Kounatidis, I., Chtarbanova, S., Cao, Y., Hayne, M., Jayanth, D., Ganetzky, B., and
702 Ligoxygakis, P. (2017). NF-kappaB Immunity in the Brain Determines Fly
703 Lifespan in Healthy Aging and Age-Related Neurodegeneration. Cell Rep *19*, 836-
704 848.
705 Kulshammer, E., Mundorf, J., Kilinc, M., Frommolt, P., Wagle, P., and Uhlirova, M.
706 (2015). Interplay among Drosophila transcription factors Ets21c, Fos and Ftz-F1
707 drives JNK-mediated tumor malignancy. Dis Model Mech *8*, 1279-1293.
708 Lemaitre, B., Nicolas, E., Michaut, L., Reichhart, J.M., and Hoffmann, J.A. (1996).
709 The dorsoventral regulatory gene cassette spatzle/Toll/cactus controls the
710 potent antifungal response in Drosophila adults. Cell *86*, 973-983.
711 Leulier, F., Rodriguez, A., Khush, R.S., Abrams, J.M., and Lemaitre, B. (2000). The
712 Drosophila caspase Dredd is required to resist gram-negative bacterial infection.
713 EMBO Rep *1*, 353-358.
714 Levashina, E.A., Ohresser, S., Bulet, P., Reichhart, J.M., Hetru, C., and Hoffmann, J.A.
715 (1995). Metchnikowin, a novel immune-inducible proline-rich peptide from

716 Drosophila with antibacterial and antifungal properties. Eur J Biochem *233*, 694-
717 700.
718 Lezi, E., Zhou, T., Koh, S., Chuang, M., Sharma, R., Pujol, N., Chisholm, A.D., Eroglu,
719 C., Matsunami, H., and Yan, D. (2018). An Antimicrobial Peptide and Its Neuronal
720 Receptor Regulate Dendrite Degeneration in Aging and Infection. Neuron *97*,
721 125-138 e125.
722 Mergaert, P., Kikuchi, Y., Shigenobu, S., and Nowack, E.C.M. (2017). Metabolic
723 Integration of Bacterial Endosymbionts through Antimicrobial Peptides. Trends
724 Microbiol *25*, 703-712.
725 Moreno, E., Yan, M., and Basler, K. (2002). Evolution of TNF signaling
726 mechanisms: JNK-dependent apoptosis triggered by Eiger, the Drosophila
727 homolog of the TNF superfamily. Curr Biol *12*, 1263-1268.
728 Parameswaran, N., and Patial, S. (2010). Tumor Necrosis Factor-α Signaling in
729 Macrophages. Crit Rev Eukaryot Gene Expr *20*, 87-103.
730 Parisi, F., Stefanatos, R.K., Strathdee, K., Yu, Y., and Vidal, M. (2014). Transformed
731 epithelia trigger non-tissue-autonomous tumor suppressor response by
732 adipocytes via activation of Toll and Eiger/TNF signaling. Cell Rep *6*, 855-867.
733 Parvy, J.P., Hodgson, J.A., and Cordero, J.B. (2018). Drosophila as a Model System
734 to Study Nonautonomous Mechanisms Affecting Tumour Growth and Cell Death.
735 Biomed Res Int *2018*, 7152962.
736 Pastor-Pareja, J.C., Grawe, F., Martin-Blanco, E., and Garcia-Bellido, A. (2004).
737 Invasive cell behavior during Drosophila imaginal disc eversion is mediated by
738 the JNK signaling cascade. Dev Cell *7*, 387-399.
739 Riedl, S., Rinner, B., Asslaber, M., Schaider, H., Walzer, S., Novak, A., Lohner, K.,
740 and Zweytick, D. (2011). In search of a novel target - phosphatidylserine exposed
741 by non-apoptotic tumor cells and metastases of malignancies with poor
742 treatment efficacy. Biochim Biophys Acta *1808*, 2638-2645.
743 Santabarbara-Ruiz, P., Lopez-Santillan, M., Martinez-Rodriguez, I., Binagui-Casas,
744 A., Perez, L., Milan, M., Corominas, M., and Serras, F. (2015). ROS-Induced JNK
745 and p38 Signaling Is Required for Unpaired Cytokine Activation during
746 Drosophila Regeneration. PLoS Genet *11*, e1005595.
747 Shafee, T.M., Lay, F.T., Phan, T.K., Anderson, M.A., and Hulett, M.D. (2017).
748 Convergent evolution of defensin sequence, structure and function. Cell Mol Life
749 Sci *74*, 663-682.
750 Shklyar, B., Levy-Adam, F., Mishnaevski, K., and Kurant, E. (2013). Caspase
751 activity is required for engulfment of apoptotic cells. Mol Cell Biol *33*, 3191-3201.
752 Srivastava, A., Pastor-Pareja, J.C., Igaki, T., Pagliarini, R., and Xu, T. (2007).
753 Basement membrane remodeling is essential for Drosophila disc eversion and
754 tumor invasion. Proc Natl Acad Sci U S A *104*, 2721-2726.
755 Sun, C.Q., Arnold, R., Fernandez-Golarz, C., Parrish, A.B., Almekinder, T., He, J., Ho,
756 S.M., Svoboda, P., Pohl, J., Marshall, F.F.*, et al.* (2006). Human beta-defensin-1, a
757 potential chromosome 8p tumor suppressor: control of transcription and
758 induction of apoptosis in renal cell carcinoma. Cancer Res *66*, 8542-8549.
759 Teng, M.W., Swann, J.B., Koebel, C.M., Schreiber, R.D., and Smyth, M.J. (2008).
760 Immune-mediated dormancy: an equilibrium with cancer. J Leukoc Biol *84*, 988-
761 993.
762 Tjabringa, G.S., Aarbiou, J., Ninaber, D.K., Drijfhout, J.W., Sorensen, O.E.,
763 Borregaard, N., Rabe, K.F., and Hiemstra, P.S. (2003). The antimicrobial peptide
764 LL-37 activates innate immunity at the airway epithelial surface by

765 transactivation of the epidermal growth factor receptor. J Immunol *171*, 6690-
766 6696.
767 Tokumaru, S., Sayama, K., Shirakata, Y., Komatsuzawa, H., Ouhara, K., Hanakawa,
768 Y., Yahata, Y., Dai, X., Tohyama, M., Nagai, H., *et al.* (2005). Induction of
769 keratinocyte migration via transactivation of the epidermal growth factor
770 receptor by the antimicrobial peptide LL-37. J Immunol *175*, 4662-4668.
771 Tung, T.T., Nagaosa, K., Fujita, Y., Kita, A., Mori, H., Okada, R., Nonaka, S., and
772 Nakanishi, Y. (2013). Phosphatidylserine recognition and induction of apoptotic
773 cell clearance by Drosophila engulfment receptor Draper. J Biochem *153*, 483-
774 491.
775 Tzou, P., De Gregorio, E., and Lemaitre, B. (2002). How Drosophila combats
776 microbial infection: a model to study innate immunity and host-pathogen
777 interactions. Curr Opin Microbiol *5*, 102-110.
778 Tzou, P., Ohresser, S., Ferrandon, D., Capovilla, M., Reichhart, J.M., Lemaitre, B.,
779 Hoffmann, J.A., and Imler, J.L. (2000). Tissue-specific inducible expression of
780 antimicrobial peptide genes in Drosophila surface epithelia. Immunity *13*, 737-
781 748.
782 Uhlirova, M., and Bohmann, D. (2006). JNK- and Fos-regulated Mmp1 expression
783 cooperates with Ras to induce invasive tumors in Drosophila. EMBO J *25*, 5294-
784 5304.
785 van Wetering, S., Mannesse-Lazeroms, S.P., van Sterkenburg, M.A., and Hiemstra,
786 P.S. (2002). Neutrophil defensins stimulate the release of cytokines by airway
787 epithelial cells: modulation by dexamethasone. Inflamm Res *51*, 8-15.
788 Wang, C., Chen, Y.W., Zhang, L., Gong, X.G., Zhou, Y., and Shang, D.J. (2016).
789 Melanoma cell surface-expressed phosphatidylserine as a therapeutic target for
790 cationic anticancer peptide, temporin-1CEa. J Drug Target *24*, 548-556.
791 Wang, C., Dong, S., Zhang, L., Zhao, Y., Huang, L., Gong, X., Wang, H., and Shang, D.
792 (2017). Cell surface binding, uptaking and anticancer activity of L-K6, a
793 lysine/leucine-rich peptide, on human breast cancer MCF-7 cells. Sci Rep *7*, 8293.
794 Wilson, C.L., Ouellette, A.J., Satchell, D.P., Ayabe, T., Lopez-Boado, Y.S., Stratman,
795 J.L., Hultgren, S.J., Matrisian, L.M., and Parks, W.C. (1999). Regulation of intestinal
796 alpha-defensin activation by the metalloproteinase matrilysin in innate host
797 defense. Science *286*, 113-117.
798 Wilson, C.L., Schmidt, A.P., Pirila, E., Valore, E.V., Ferri, N., Sorsa, T., Ganz, T., and
799 Parks, W.C. (2009). Differential Processing of {alpha}- and {beta}-Defensin
800 Precursors by Matrix Metalloproteinase-7 (MMP-7). J Biol Chem *284*, 8301-8311.
801 Ye, Z., Dong, H., Li, Y., Ma, T., Huang, H., Leong, H.S., Eckel-Passow, J., Kocher, J.A.,
802 Liang, H., and Wang, L. (2018). Prevalent Homozygous Deletions of Type I
803 Interferon and Defensin Genes in Human Cancers Associate with
804 Immunotherapy Resistance. Clin Cancer Res *24*, 3299-3308.
805 Yeaman, M.R., and Yount, N.Y. (2003). Mechanisms of antimicrobial peptide
806 action and resistance. Pharmacol Rev *55*, 27-55.
807 Zhao, H.W., Zhou, D., and Haddad, G.G. (2011). Antimicrobial peptides increase
808 tolerance to oxidant stress in Drosophila melanogaster. J Biol Chem *286*, 6211-
809 6218.
810 Zhu, M., Xin, T., Weng, S., Gao, Y., Zhang, Y., Li, Q., and Li, M. (2010). Activation of
811 JNK signaling links lgl mutations to disruption of the cell polarity and epithelial
812 organization in Drosophila imaginal discs. Cell Res *20*, 242-245.
813

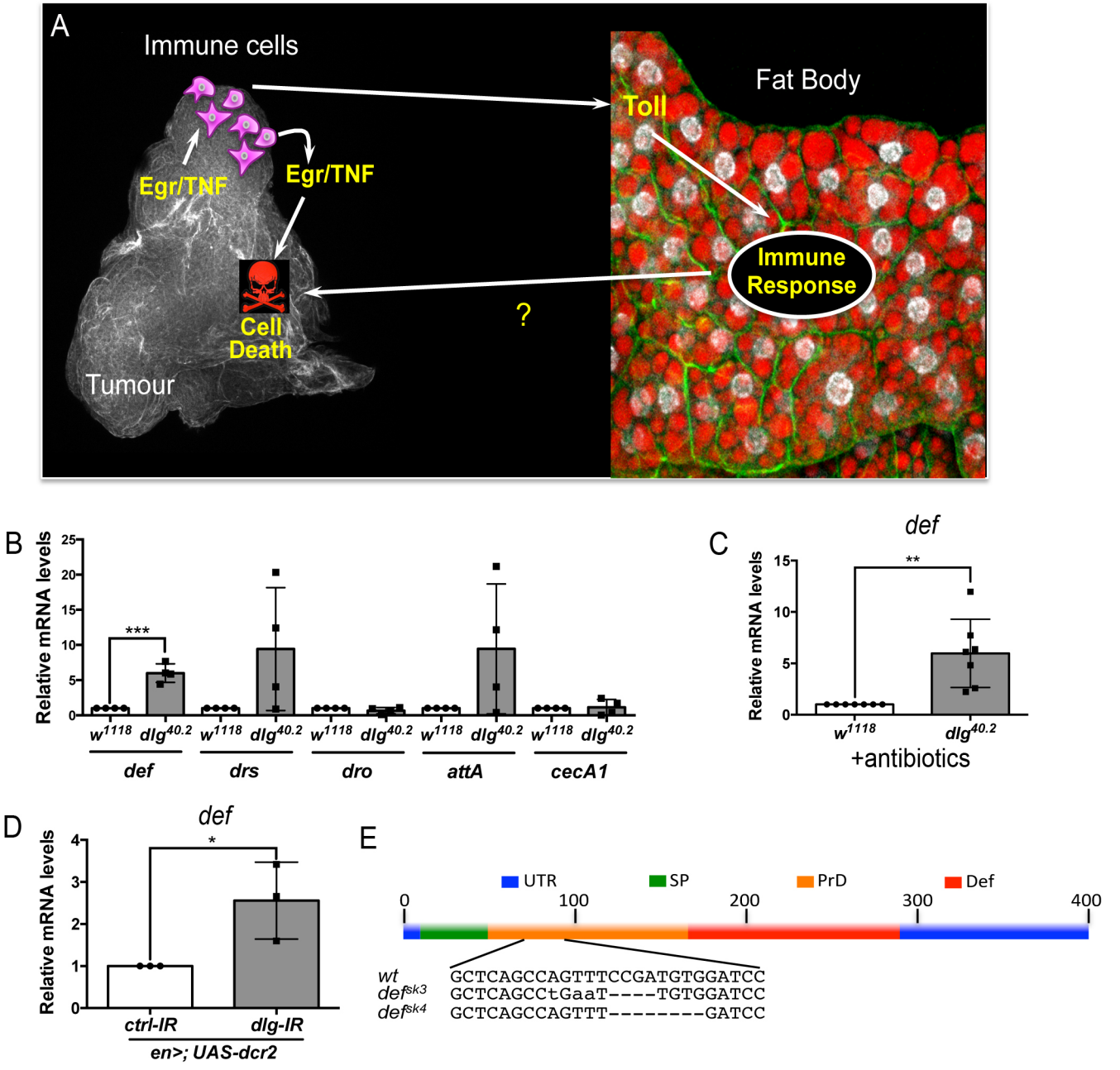
A
Immune cells
Egr/TNF
Egr/TNF
Cell Death
Tumour
Fat Body
Toll
Immune Response
?
B
Relative mRNA levels
***
w1118
dlg40.2
def
drs
dro
attA
cecA1
C
def
**
+antibiotics
D
def
*
ctrl-IR
dlg-IR
en>; UAS-dcr2
E
UTR
SP
PrD
Def
0
100
200
300
400
wt GCTCAGCCAGTTTCCGATGTGGATCC
defsk3 GCTCAGCCtGaaT----TGTGGATCC
defsk4 GCTCAGCCAGTTT--------GATCC

**Figure 1**

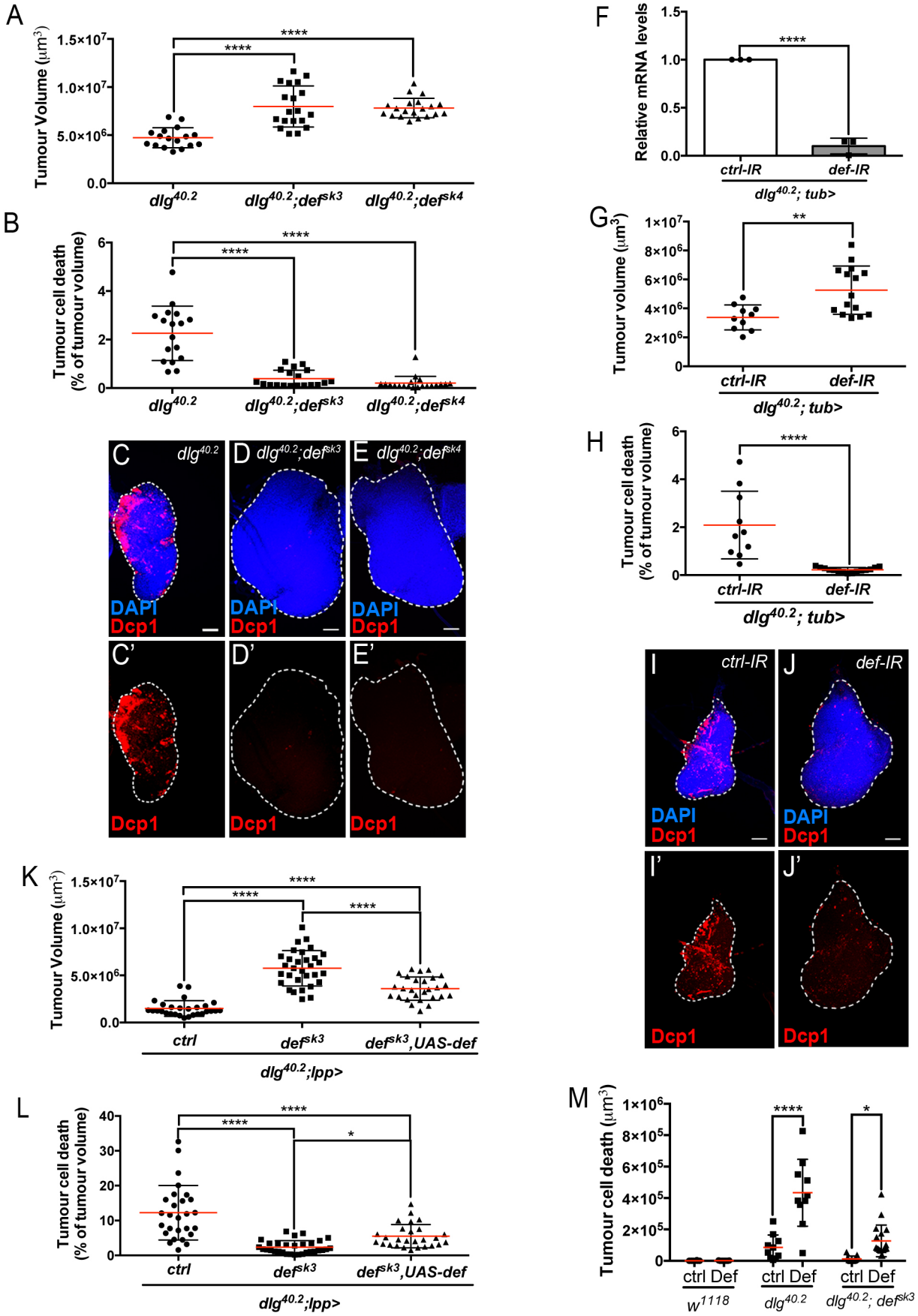
A
Tumour Volume (μm³)
1.5×10⁷
1.0×10⁷
5.0×10⁶
0.0
****
****
dlg40.2
dlg40.2;defsk3
dlg40.2;defsk4
B
Tumour cell death (% of tumour volume)
6
4
2
0
****
****
dlg40.2
dlg40.2;defsk3
dlg40.2;defsk4
C
dlg40.2
D
dlg40.2;defsk3
E
dlg40.2;defsk4
DAPI
Dcp1
C'
D'
E'
Dcp1
F
Relative mRNA levels
1.5
1.0
0.5
0.0
****
ctrl-IR
def-IR
dlg40.2; tub>
G
Tumour volume (μm³)
1×10⁷
8×10⁶
6×10⁶
4×10⁶
2×10⁶
0
**
ctrl-IR
def-IR
dlg40.2; tub>
H
Tumour cell death (% of tumour volume)
6
4
2
0
****
ctrl-IR
def-IR
dlg40.2; tub>
I
ctrl-IR
J
def-IR
DAPI
Dcp1
I'
J'
Dcp1
K
Tumour Volume (μm³)
1.5×10⁷
1.0×10⁷
5.0×10⁶
0.0
****
****
****
ctrl
defsk3
defsk3,UAS-def
dlg40.2;lpp>
L
Tumour cell death (% of tumour volume)
40
30
20
10
0
****
****
*
ctrl
defsk3
defsk3,UAS-def
dlg40.2;lpp>
M
Tumour cell death (μm³)
1×10⁶
8×10⁵
6×10⁵
4×10⁵
2×10⁵
0
****
*
ctrl Def
ctrl Def
ctrl Def
w1118
dlg40.2
dlg40.2; defsk3

**Figure 2**

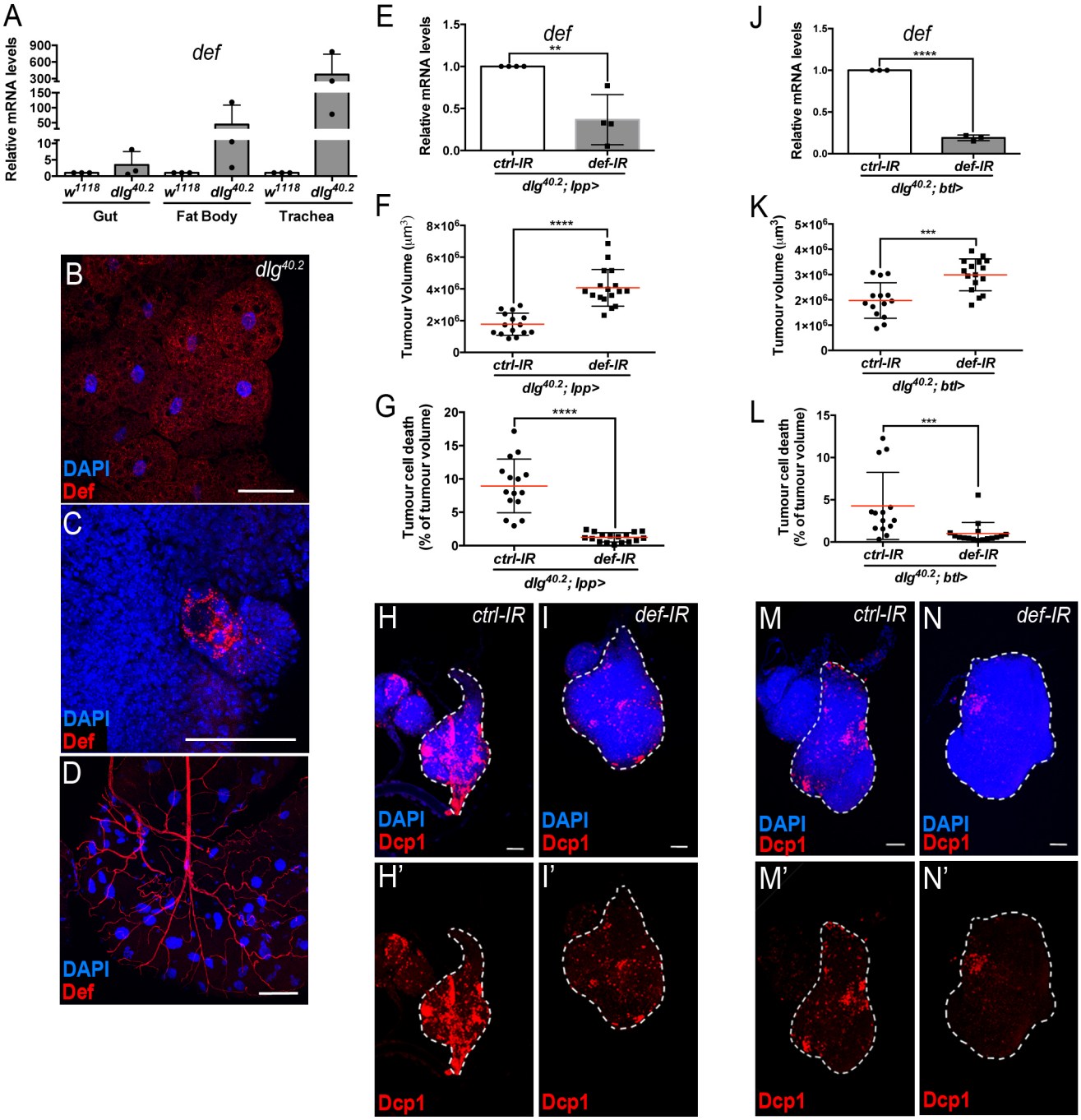
A
def
Relative mRNA levels
900
600
300
150
100
50
10
5
0
w1118
dlg40.2
w1118
dlg40.2
w1118
dlg40.2
Gut
Fat Body
Trachea
B
dlg40.2
DAPI
Def
C
DAPI
Def
D
DAPI
Def
E
def
Relative mRNA levels
1.5
1.0
0.5
0.0
**
ctrl-IR
def-IR
dlg40.2; lpp>
F
Tumour Volume (µm3)
8×106
6×106
4×106
2×106
0
****
ctrl-IR
def-IR
dlg40.2; lpp>
G
Tumour cell death
(% of tumour volume)
20
15
10
5
0
****
ctrl-IR
def-IR
dlg40.2; lpp>
J
def
Relative mRNA levels
1.5
1.0
0.5
0.0
****
ctrl-IR
def-IR
dlg40.2; btl>
K
Tumour volume (µm3)
5×106
4×106
3×106
2×106
1×106
0
***
ctrl-IR
def-IR
dlg40.2; btl>
L
Tumour cell death
(% of tumour volume)
15
10
5
0
***
ctrl-IR
def-IR
dlg40.2; btl>
H
ctrl-IR
DAPI
Dcp1
I
def-IR
DAPI
Dcp1
H'
Dcp1
I'
Dcp1
M
ctrl-IR
DAPI
Dcp1
N
def-IR
DAPI
Dcp1
M'
Dcp1
N'
Dcp1

**Figure 3**

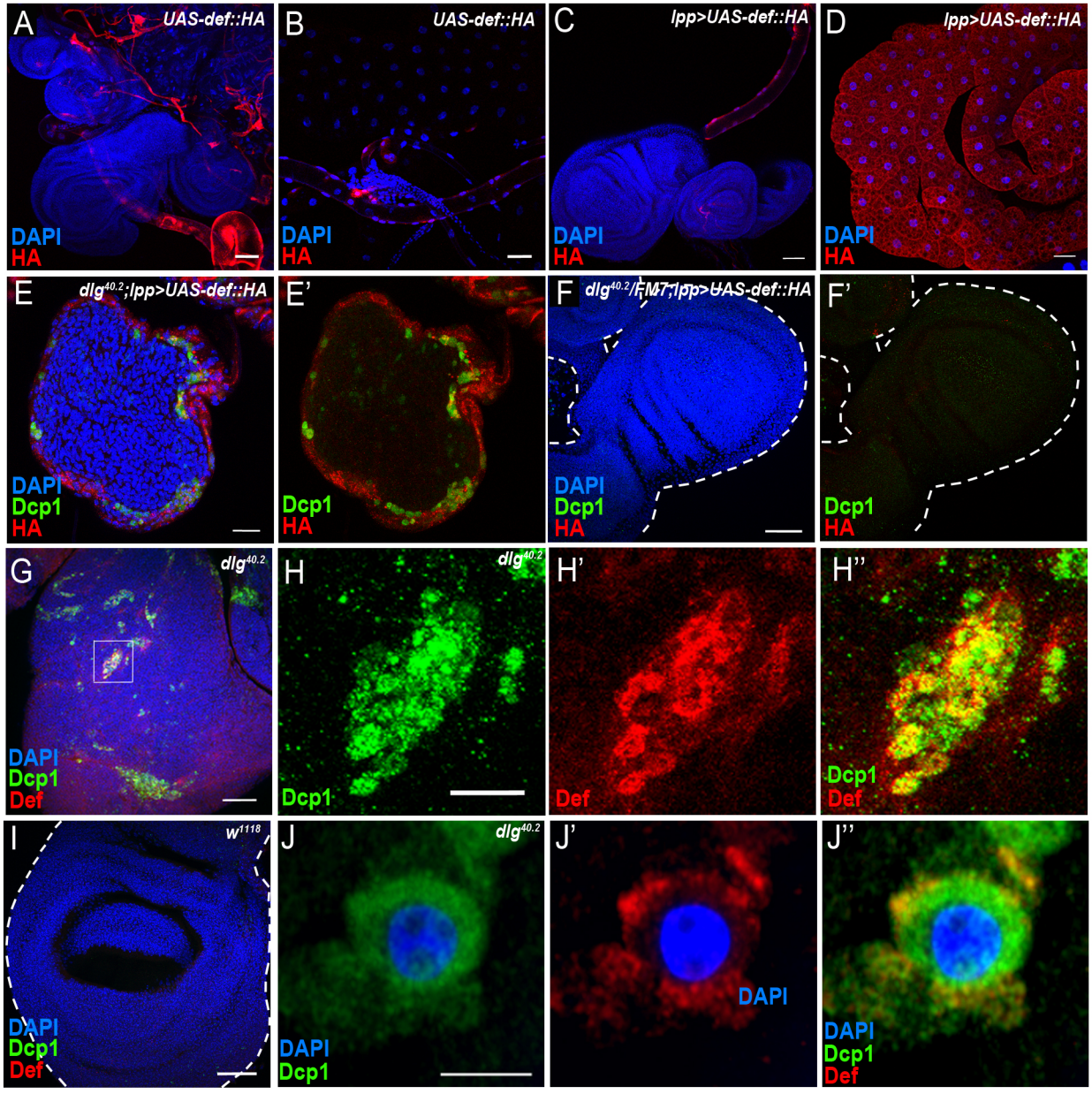
A
UAS-def::HA
DAPI
HA
B
UAS-def::HA
DAPI
HA
C
lpp>UAS-def::HA
DAPI
HA
D
lpp>UAS-def::HA
DAPI
HA
E
dlg40.2;lpp>UAS-def::HA
DAPI
Dcp1
HA
E'
Dcp1
HA
F
dlg40.2/FM7;lpp>UAS-def::HA
DAPI
Dcp1
HA
F'
Dcp1
HA
G
dlg40.2
DAPI
Dcp1
Def
H
dlg40.2
Dcp1
H'
Def
H''
Dcp1
Def
I
w1118
DAPI
Dcp1
Def
J
dlg40.2
DAPI
Dcp1
J'
DAPI
J''
DAPI
Dcp1
Def

Figure 4

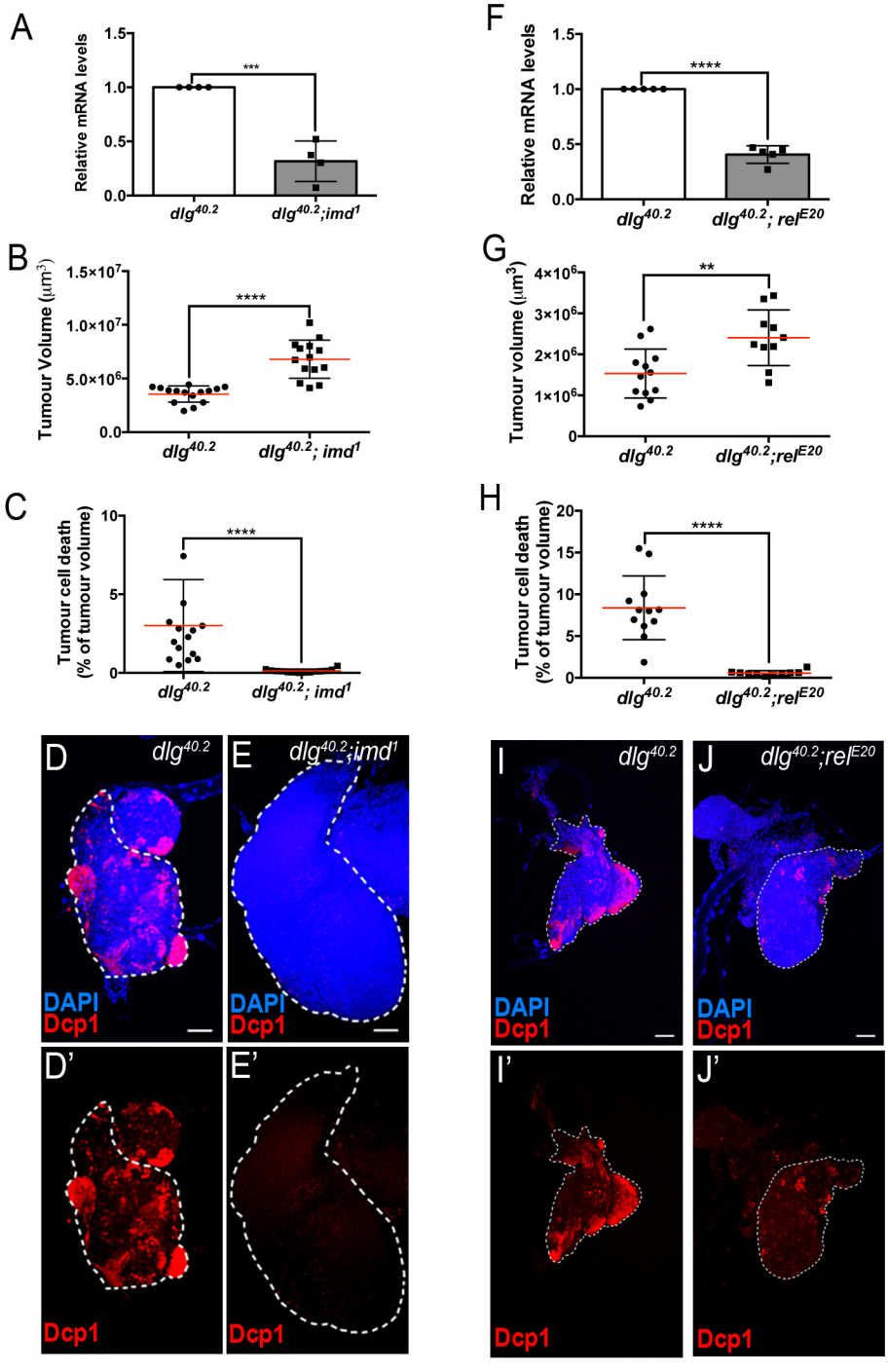
A
Relative mRNA levels
1.5
1.0
0.5
0.0
***
dlg40.2
dlg40.2;imd1
B
Tumour Volume (µm3)
1.5×107
1.0×107
5.0×106
0.0
****
dlg40.2
dlg40.2; imd1
C
Tumour cell death (% of tumour volume)
10
5
0
****
dlg40.2
dlg40.2; imd1
F
Relative mRNA levels
1.5
1.0
0.5
0.0
****
dlg40.2
dlg40.2; relE20
G
Tumour volume (µm3)
4×106
3×106
2×106
1×106
0
**
dlg40.2
dlg40.2;relE20
H
Tumour cell death (% of tumour volume)
20
15
10
5
0
****
dlg40.2
dlg40.2;relE20
D
dlg40.2
DAPI
Dcp1
E
dlg40.2;imd1
DAPI
Dcp1
D'
Dcp1
E'
Dcp1
I
dlg40.2
DAPI
Dcp1
J
dlg40.2;relE20
DAPI
Dcp1
I'
Dcp1
J'
Dcp1

**Figure 5**

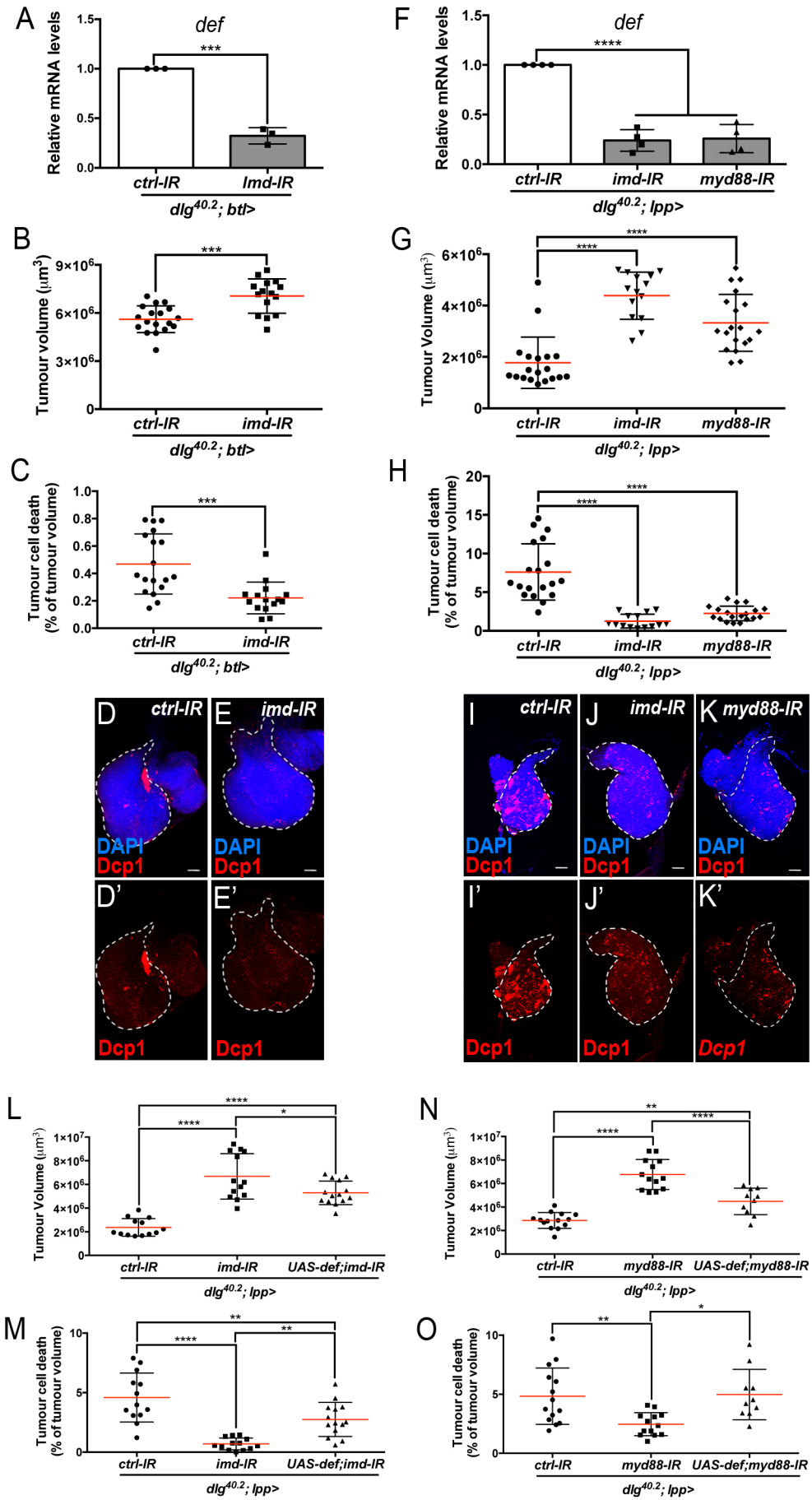
A
def
Relative mRNA levels
1.5
1.0
0.5
0.0
***
ctrl-IR
Imd-IR
dlg40.2; btl>
B
Tumour volume (µm3)
9×106
6×106
3×106
0
***
ctrl-IR
imd-IR
dlg40.2; btl>
C
Tumour cell death (% of tumour volume)
1.0
0.8
0.6
0.4
0.2
0.0
***
ctrl-IR
imd-IR
dlg40.2; btl>
F
def
Relative mRNA levels
1.5
1.0
0.5
0.0
****
ctrl-IR
imd-IR
myd88-IR
dlg40.2; lpp>
G
Tumour Volume (µm3)
6×106
4×106
2×106
0
****
****
ctrl-IR
imd-IR
myd88-IR
dlg40.2; lpp>
H
Tumour cell death (% of tumour volume)
20
15
10
5
0
****
****
ctrl-IR
imd-IR
myd88-IR
dlg40.2; lpp>
D ctrl-IR
E imd-IR
DAPI
Dcp1
D'
E'
Dcp1
I ctrl-IR
J imd-IR
K myd88-IR
I'
J'
K'
L
Tumour Volume (µm3)
1×107
8×106
6×106
4×106
2×106
0
****
****
*
ctrl-IR
imd-IR
UAS-def;imd-IR
dlg40.2; lpp>
N
Tumour Volume (µm3)
**
****
****
ctrl-IR
myd88-IR
UAS-def;myd88-IR
dlg40.2; lpp>
M
Tumour cell death (% of tumour volume)
10
5
0
**
****
**
ctrl-IR
imd-IR
UAS-def;imd-IR
dlg40.2; lpp>
O
Tumour cell death (% of tumour volume)
10
5
0
**
*
ctrl-IR
myd88-IR
UAS-def;myd88-IR
dlg40.2; lpp>

**Figure 6**

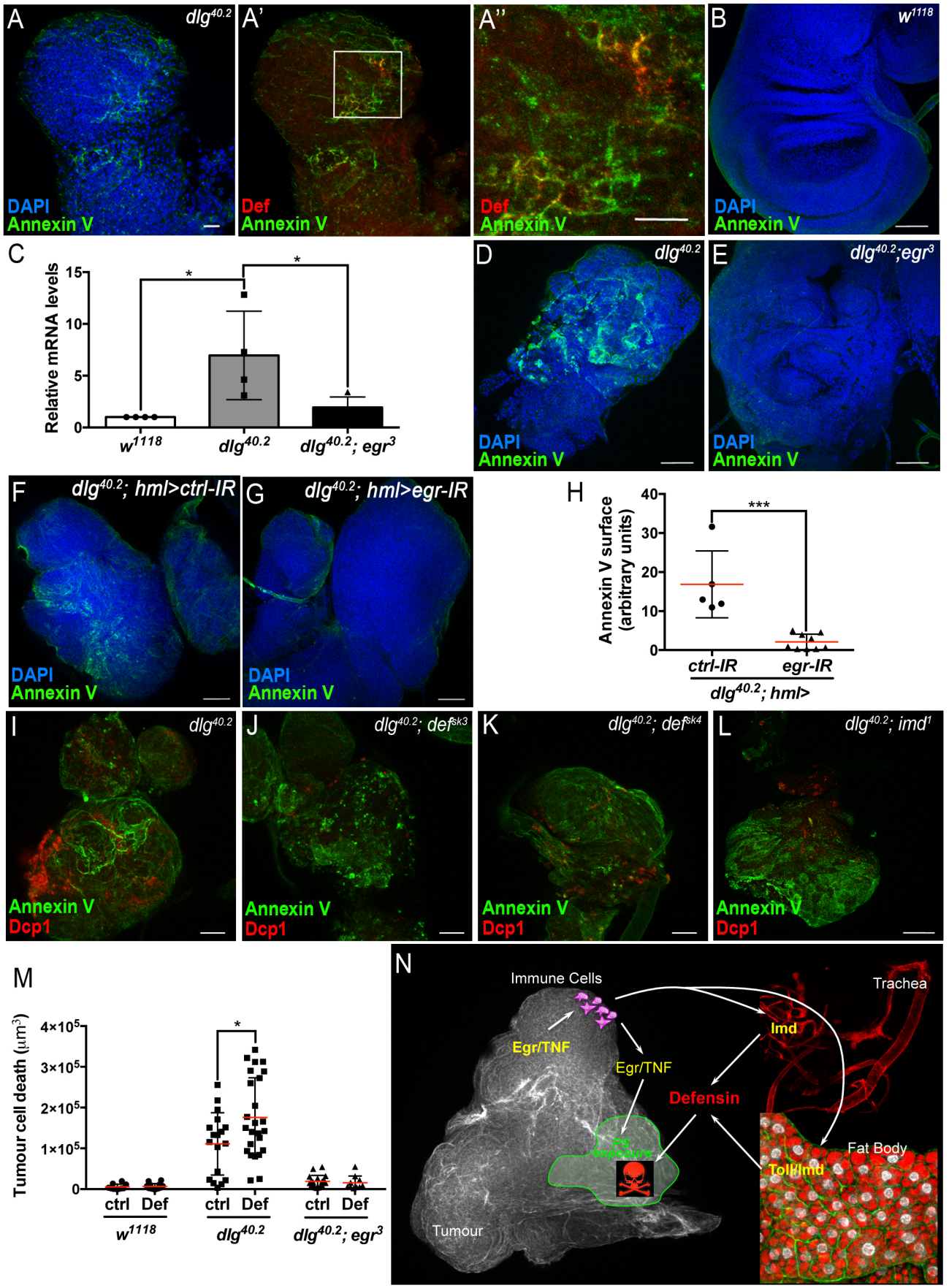
A
dlg40.2
DAPI
Annexin V
A'
Def
Annexin V
A''
Def
Annexin V
B
w1118
DAPI
Annexin V
C
Relative mRNA levels
15
10
5
0
*
*
w1118
dlg40.2
dlg40.2; egr3
D
dlg40.2
DAPI
Annexin V
E
dlg40.2;egr3
DAPI
Annexin V
F
dlg40.2; hml>ctrl-IR
DAPI
Annexin V
G
dlg40.2; hml>egr-IR
DAPI
Annexin V
H
Annexin V surface (arbitrary units)
40
30
20
10
0
***
ctrl-IR
egr-IR
dlg40.2; hml>
I
dlg40.2
Annexin V
Dcp1
J
dlg40.2; defsk3
Annexin V
Dcp1
K
dlg40.2; defsk4
Annexin V
Dcp1
L
dlg40.2; imd1
Annexin V
Dcp1
M
Tumour cell death (μm3)
4×105
3×105
2×105
1×105
0
*
ctrl
Def
ctrl
Def
ctrl
Def
w1118
dlg40.2
dlg40.2; egr3
N
Immune Cells
Trachea
Egr/TNF
Egr/TNF
Imd
Defensin
Fat Body
Toll/Imd
Tumour

Figure 7

## Figure Legends

**Figure 1 | *def* is induced in *dlg* mutant tumour bearing animals.** A, Working model showing the cooperation between haemocyte-derived TNF and the immune response in the fat body in tumour cell death (Parisi et al, 2014). B, RT-qPCR analyses showing expression of several AMPs in the fat body of $dlg^{40.2}$ mutant tumour bearing larvae compared to wild-type ($w^{1118}$) larvae (n=4). C, RT-qPCR analysis of *def* expression in $w^{1118}$ and $dlg^{40.2}$ whole larvae reared on antibiotics (n=7). D, RT-qPCR analysis showing *def* expression in larvae expressing a *ctrl-IR* or a *dlg-IR* in the posterior part of the wing disc (*en>;UAS-dcr2*) (n=3). E, Schematic representation of the *def* gene locus showing mutant alleles generated (UTR: Untranslated Regions, SP: Signal Peptide, PrD: Pro-Domain, Def: Mature Defensin). Statistical analysis: B-D, Student t-test, B, ***p=0.0003, C, **p=0.0074, D, *p=0.042.

**Figure 2 | Def restricts tumour growth and promotes tumour cell death.**
A-E', Quantification of tumour volume (TV) (A) and tumour cell death (TCD) (B) in wing imaginal discs from $dlg^{40.2}$ (n=17), $dlg^{40.2};def^{sk3}$ (n=19) and $dlg^{40.2};def^{sk4}$ (n=20) mutant larvae and representative immunofluorescence images of tissues quantified (C-E'). F, RT-qPCR analysis showing *def* expression upon ubiquitous knockdown ($dlg^{40.2}$*; tub>*) (n=3). G-J', Quantification of TV (G) and TCD (H) in wing imaginal discs from larvae ubiquitously expressing a *control-IR* (*ctrl-IR*: n=10) or a *def-IR* (n=15) and representative immunofluorescence images of tissues quantified (I-J'). K-L, Quantification of TV (G) and TCD (H) in wing imaginal discs from *dlg* mutant controls ($dlg^{40.2}$*;lpp>*: n=28), *dlg;*$def^{sk3}$ mutants controls ($dlg^{40.2};def^{sk3}$*;lpp>*: n=31) or *dlg;*$def^{sk3}$ mutants expressing *def* in the fat body ($dlg^{40.2};def^{sk3}$*,UAS-def;lpp>*: n=27). M, Effect of PBS (ctrl) or synthetic Def injection on TCD from wild-type larvae ($w^{1118}$, ctrl: n=10, Def: n=9), $dlg^{40.2}$ (ctrl: n=10, Def: n=10) and $dlg^{40.2};def^{sk3}$ (ctrl: n=11, Def: n=18) mutant larvae. Tissues were stained with 4',6-diamidino-2-phenylindole (DAPI, blue) for nuclei visualization and with anti-cleaved Decapping protein 1 (Dcp1) antibody (red) to detect apoptotic cell death. Scale bars=50 µm. Statistical analysis: A, B, K, N, One way ANOVA, *p<0.05, ****p<0.0001; F, Student t-test, ****p<0.0001, G-H, Mann-Whitney test, G, **p=0.0054, H, ****p<0.0001; M, Two way ANOVA (only relevant significant statistics are indicated), *p<0.05, ****p<0.0001.

**Figure 3 | Def from the trachea and the fat body mediates tumour cell death.** A, RT-qPCR analysis of *def* expression in gut, fat body and trachea dissected from $w^{1118}$ or $dlg^{40.2}$ mutant larvae (n=3). B-D, Fat body (B) tumour associated (C) and tumour distant trachea (D) from $dlg^{40.2}$ mutant larvae stained with DAPI (blue) and anti-Def antibody (red). E, RT-qPCR analysis of *def* expression from $dlg^{40.2}$ mutant larvae ($dlg^{40.2}$*;lpp>*) expressing a *ctrl-IR* or *def-IR* in the fat body (n=4). F-I', Quantification of TV (F) and TCD (G) in wing imaginal discs from $dlg^{40.2}$ mutant larvae ($dlg^{40.2}$*;lpp>*) expressing a *ctrl-IR* (n=15) or *def-IR* (n=17) in the fat body and representative immunofluorescence images of tissues quantified (H-I'). J, RT-qPCR analysis of *def* expression from $dlg^{40.2}$ mutant larvae ($dlg^{40.2}$*;btl>*) expressing a *ctrl-IR* or *def-IR* in the trachea (n=3). K-N', Quantification of TV (K) and TCD (L) in wing imaginal discs from $dlg^{40.2}$ mutant larvae ($dlg^{40.2}$*;btl>*) expressing a *ctrl-IR* (n=14) or *def-IR* (n=16) in the trachea and representative immunofluorescence images of tissues quantified (M-N'). Tumours were stained with DAPI (blue) and anti-Dcp1 antibody (red). Scale bars=50 µm. Statistical analysis: A, E, J, Student t-test, E, **p=0.0054, J, ****p<0.0001; F, G, K, L, Mann-Whitney test, F, G, ****p<0.0001, K, ***p=0.0009, L, ***p=0.0004.

**Figure 4 | Def from the fat body and the trachea associates with dying tumour cells.** A-B, DAPI (blue) and anti-HA antibody (red) staining showing leakiness of the def-HA construct in trachea of the *UAS-def-HA* larvae. C-D, DAPI (blue) and anti-HA antibody (red) staining showing expression of a *UAS-def-HA* transgene in the fat body and the trachea when driven with a fat body specific driver (*lpp>UAS-def-HA*). E-E', DAPI (white), anti-Dcp1 (green) and anti-HA antibody (red) staining of $dlg^{40.2}$ mutant tumour from larvae expressing the *def-HA* construct in the fat body and the trachea ($dlg^{40.2}$*;lpp>UAS-def-HA*). F-F', DAPI (white), anti-Dcp1 (green) and anti-HA antibody (red) staining of $dlg^{40.2}$ heterozygous wing disc from larvae expressing the *def-HA* construct in the fat body ($dlg^{40.2}$*/FM7;lpp>UAS-def-HA*). G-H'', $dlg^{40.2}$ mutant tumour stained with DAPI (blue), anti-Def (red) and anti-Dcp1 (green) antibodies. I, wild type ($w^{1118}$) wing imaginal disc stained with DAPI (blue), anti-Def (red) and anti-Dcp1 (green) antibodies. J-J'', High-resolution imaging of a single dying tumour cell stained with DAPI (blue), anti-Def (red) and anti-Dcp1 (green) antibodies. A-I, Scale bars=50 µm, J-J'', Scale bar=2.5 µm.

**Figure 5 | Imd and Toll pathway activation are required for *def* expression and Def-mediated tumour cell death.** A, RT-qPCR analysis of *def* expression from $dlg^{40.2}$ and $dlg^{40.2}$;$imd^{1}$ mutant larvae (n=4). B-E', Quantification of TV (B) and TCD (C) in wing imaginal discs from $dlg^{40.2}$ (n=15) and $dlg^{40.2}$;$imd^{1}$ (n=14) mutants larvae and representative immunofluorescence images of tissues quantified stained with DAPI (blue) and anti-Dcp1 antibody (red) (D-E'). F, RT-qPCR analysis showing *def* expression in $dlg^{40.2}$ and $dlg^{40.2}$; $rel^{E20}$ mutant animals (n=5). G-J', Quantification of TV (G) and TCD (H) from $dlg^{40.2}$ (n=12) and $dlg^{40.2}$;$rel^{E20}$ (n=10) mutant larvae and representative pictures of the corresponding tumours (I-J'). Scale bars=50 µm. Statistical analysis: A, F, Student t-test, A, ***p<0.0003, F, ****p<0.0001; B, C, G, H, Mann-Whitney test, B, C, H, ****p<0.0001, G, **p=0.009.

**Figure 6 | Imd and Toll pathway activation are required in the trachea and the fat body.** A, RT-qPCR analysis of *def* expression from $dlg^{40.2}$ mutant larvae ($dlg^{40.2}$;*btl*>) expressing a *ctrl-IR* or *imd-IR* in the trachea (n=3). B-E', Quantification of TV (B) and TCD (C) from $dlg^{40.2}$ mutant larvae ($dlg^{40.2}$;*btl*>) expressing a *ctrl-IR* (n=18) or *imd-IR* (n=15) in the trachea and representative immunofluorescence images of tissues quantified stained with DAPI (blue) and anti-Dcp1 antibody (red) (D-E'). F, RT-qPCR analysis of *def* expression from $dlg^{40.2}$ mutant larvae ($dlg^{40.2}$;*lpp*>) expressing a *ctrl-IR*, an *imd-IR* or a myd88-IR in the fat body. G-K', Quantification of TV (G) and TCD (H) from $dlg^{40.2}$ mutant larvae ($dlg^{40.2}$;*lpp*>) expressing a *ctrl-IR*, an *imd-IR* or a myd88-IR in the fat body and representative immunofluorescence images of tissues quantified (I-K'). L-O, Quantification of TV (L, N) and TCD (M, O) from $dlg^{40.2}$ mutant larvae ($dlg^{40.2}$;*lpp*>) expressing a *ctrl-IR*, an *imd-IR* alone or in combination with a *UAS-def* in the fat body (L, M) and from $dlg^{40.2}$ mutant larvae ($dlg^{40.2}$;*lpp*>) expressing a *ctrl-IR*, a *myd88-IR* alone or in combination with a *UAS-def* in the fat body (N, O). Scale bars=50 µm. Statistical analysis: A, Student t-test, A, ***p=0.0001; B, C, Mann-Whitney test, B, ***p=0.0003, C, ***p=0.0002; F, G, H, L-O, One way ANOVA, *p<0.05, **p<0.01, ****p<0.0001.

**Figure 7 | TNF is required for PS exposure and Defensin-driven tumour cell death.** A-A'', DAPI (blue), Annexin V (green) and anti-Def (red) staining of $dlg^{40.2}$ mutant tumours. B, D, E, Annexin V (green) and DAPI (blue) staining of wing

imaginal discs from larvae of the indicated genotypes. C, RT-qPCR analysis showing *def* expression in wild-type, $dlg^{40.2}$ or $dlg^{40.2};egr^{3}$ mutants. F, G, Annexin V (green) and DAPI (blue) staining of wing imaginal discs from *dlg* mutant larvae ($dlg^{40.2}$,*hml*>) expressing a *ctrl-IR* (n=5) or an *egr-IR* (n=9) in the haemocytes. H, Quantification of Annexin V signal on tumours from the corresponding genotypes. I-L, Annexin V (green) and anti-Dcp1 (red) antibody staining of tumours from $dlg^{40.2}$, $dlg^{40.2};def^{sk3}$, $dlg^{40.2};def^{sk4}$ and $dlg^{40.2}$ mutant larvae. M, Quantification of TCD upon PBS (ctrl) or Def injection in wild-type ($w^{1118}$, ctrl: n=10, Def: n=14), $dlg^{40.2}$ (ctrl/Def: n=18) or $dlg^{40.2};egr^{3}$ (ctrl: n=20, Def: n=13) mutant larvae. N, A model for Def antitumoural activity. Scale bars=50 µm. Statistical analysis: C, One way ANOVA, *p<0.05; H, Mann-Whitney test, ***p=0.001; M, Two way ANOVA (only relevant significant statistics are indicated), **p<0.01.